Critical Current Reduction of Field-Free Perpendicular SOT-MTJ by STT Assist Using Micromagnetic Simulation

Wei-Jen Chen[1], Ya-Jui Tsou[1], Huan-Chi Shih[1], Pang-Chun Liu[2], and C. W. Liu[1,2,*]
[1]Graduate Institute of Electronics Engineering, National Taiwan University, Taipei, Taiwan
[2]Graduate Institute of Photonics and Optoelectronics, National Taiwan University, Taipei, Taiwan
*Email: cliu@ntu.edu.tw

***Abstract*—Field-free switching of perpendicular spin-orbit torque magnetic tunnel junction (p-SOT-MTJ) is investigated using micromagnetic simulation to evaluate the SOT critical current density ($J_{C, SOT}$). The spin-transfer torque (STT) can break the symmetry and ensure the deterministic switching of p-SOT-MTJ without the external magnetic field. The decreasing SOT pulse width (t_{SOT}) below 1 ns causes the significant increase of $J_{C, SOT}$. The increasing STT current density (J_{STT}) can overcome the damping torque and reduce the $J_{C, SOT}$. For a short t_{SOT} of 0.2 ns, the increase of STT current density (J_{STT}) from 0.64 MA/cm^2 to 0.97 MA/cm^2 (V_{STT} from 0.2 V to 0.3 V) reduces the $J_{C, SOT}$ by 36%. As the spin Hall angle (θ_{SH}) of SOT channels increases from 0.28 to 0.5, the $J_{C, SOT}$ can further be reduced by 46%.**

***Keywords*—SOT-MRAM, MTJ, field-free switching, critical current, micromagnetic simulation**

I. Introduction

Spin-orbit torque magnetoresistive random-access memory (SOT-MRAM) is a promising candidate among the emerging memories for SRAM replacement in high level cache due to its ultra-fast switching, unlimited endurance, and low energy consumption [1]. According to the magnetization direction of SOT-MTJ, the SOT-MRAM can be divided into three types – type-X, type-Y, and type-Z [2]. For the type-X and type-Y SOT-MRAMs with the in-plane magnetization, the elliptical shape of SOT-MTJ limits the scalability. The type-Z SOT-MRAM using p-SOT-MTJ with circular shape has well-behaved scalability. Although the switching of type-Z SOT-MRAM needs the external magnetic field, methods of field-free switching have been proposed. Reportedly, the magnetic hard mask without current can generate the stray field for field-free switching [1]. The stray field may also interfere other cells in the memory array. The combination of STT and SOT effects was demonstrated as an alternative method of field-free switching [3], [4], [5]. However, the SOT-MTJ requires the large critical current density as compared to STT-MTJ. In this work, the mechanisms of STT-assisted SOT switching are studied using micromagnetic simulation for $J_{C, SOT}$ reduction. The effects of V_{STT}, t_{SOT}, and θ_{SH} on $J_{C, SOT}$ are also discussed.

II. Methodology

A. Computational setup

The schematic structure in the micromagnetic simulation is shown in **Fig. 1**. The FL, RL, and PL represent the free layer, the reference layer, and the pinned layer, respectively. The magnetization dynamics of the FL can be described by the Landau-Lifshitz-Gilbert (LLG) equations with STT and SOT effects.

Where γ, $\vec{M}_F$, $\vec{H}_{eff}$, α, H_{STT}, $\vec{M}_R$, H_{SOT}, and $\vec{\sigma}$ are

$$\frac{d\vec{M}_F(\vec{r})}{dt} = -\gamma\left(\vec{M}_F(\vec{r}) \times \vec{H}_{eff}(\vec{r})\right) + \alpha\left(\vec{M}_F(\vec{r}) \times \frac{d\vec{M}_F(\vec{r})}{dt}\right) - \gamma H_{STT}\left[\vec{M}_F(\vec{r}) \times \left(\vec{M}_R(\vec{r}) \times \vec{M}_F(\vec{r})\right)\right] - \gamma H_{SOT}\left[\vec{M}_F(\vec{r}) \times \left(\vec{M}_F(\vec{r}) \times \vec{\sigma}\right)\right] \quad (1)$$

gyromagnetic ratio, magnetization of FL, effective magnetic field, damping constant, effective magnetic field generated by STT effect, magnetization of RL, effective magnetic field generated by SOT effect, and spin index. The H_{STT} is defined by

where $\hbar$, η, J_e, e, M_s, t_F, and $cos\theta_{FL/RL}$ are Planck constant,

$$H_{STT} = \frac{\hbar \eta J_e}{2eM_s t_F(1 + cos\theta_{FL/RL})} \quad (2)$$

STT efficiency, charge current density, elementary charge, saturation magnetization, thickness of FL, and angle between FL and RL. The H_{SOT} is defined by

$$H_{SOT} = \frac{\hbar \theta_{SH} J_e}{2eM_s t_F} \quad (3)$$

where θ_{SH} is spin Hall angle of the SOT channel.

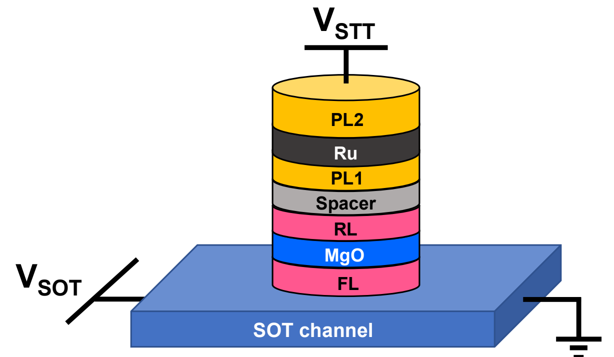

Fig. 1. Schematic structure of p-SOT-MTJ for STT-assisted SOT switching.

978-1-6654-0685-7/21/$31.00 ©2021 IEEE

B. STT-assisted SOT switching

The micromagnetic simulation is conducted using EXAMAG LLG simulator. The simulation parameters are listed in **Table I**. The V_{STT} for field-free switching is applied at the top of MTJ, and the STT pulse width (t_{STT}) is longer than the t_{SOT} to ensure the deterministic transition. At the beginning of SOT pulse, the magnetization of FL in P state is rapidly driven from H_{effz} (+ z axis) to the +y axis by SOT **(Fig. 2(a)(b))** without incubation delay. The SOT originates from the accumulation of spins at the interface between FL and SOT channel due to the spin Hall effect of the SOT channel. Note that the direction of spins ($\vec{\sigma}$) depends on the materials of SOT channel. The magnitude of SOT is determined by the θ_{SH}. The θ_{SH} represents the charge to spin conversion efficiency, which is defined as $\tan^{-1}(|J_s|/|J_e|)$. The J_s and J_e are the spin angular momentum density and the charge current density, respectively. After the SOT pulse is turned-off, the continuous STT pulse drives the magnetization toward -z axis. **(Fig. 2(c))**. When the both SOT pulse and STT pulse are turned-off, the magnetization precesses around the $\vec{H}_{effz}$ (-z axis), and the damping torque (τ_D) drives the magnetization to $\vec{H}_{effz}$ **(Fig. 2(d))**. Finally, the FL switches to the AP state **(Fig. 2(e))**. The simulated transient magnetization is shown in **Fig. 3(a)**. The small MTJ size of 40 nm results in the single domain switching **(Fig. 3(b))**, since the MTJ size is smaller than the domain wall width which is proportional to $(A_{ex}/K_{eff})^{1/2}$[10], [11].

Symbol	Description	Value
A	Exchange stiffness	20 pJ/m [5],[6]
M_s	Saturation magnetization	1.75 T (FL, RL) * 0.9 T (PL1, PL2) *
α	Damping constant	0.018 *
K_i	Interfacial anisotropy	1 mJ/m^2 [8],[9]
η	STT efficiency	0.89
D	MTJ diameter	40 nm *
t_{MgO}	MgO thickness	1.1 nm *
t_{FL}	Free layer thickness	0.9 nm *
RA	Resistance-area product	20 Ω–μm^2 *
R_P	MTJ resistance in P state	16 kΩ *
TMR	Tunnel magnetoresistance	130 % *
θ_{SH}	Spin Hall angle	0.28 *
ρ_{SOT}	SOT channel resistivity	240 μΩ–cm *
W_{SOT}	SOT channel width	500 nm *
L_{SOT}	SOT channel length	400 nm *
t_{SOT}	SOT channel thickness	12 nm *

Table I. Parameters in the micromagnetic simulation.*Values are extracted from our experimental data [7].

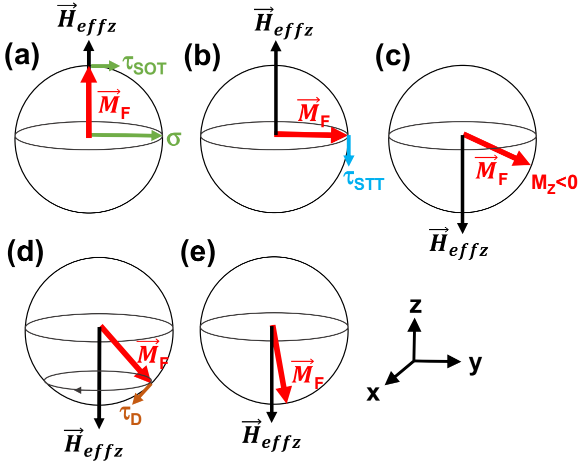

Fig. 2. Schematic magnetization dynamics of STT-assisted SOT switching without external magnetic field in the P to AP switching. (a) Initial P state. (b) Magnetization alignment to y-axis by SOT. (c) Magnetization deviation around −z axis by STT. (d) Magnetization precession around H_{eff} with the damping torque (τ_D) (V_{STT} = 0, V_{SOT} = 0). (e) Final AP state.

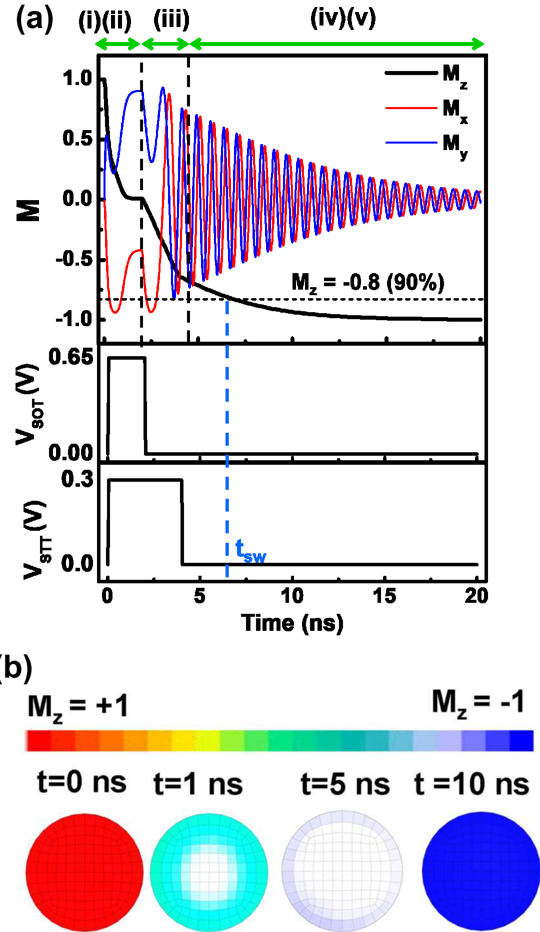

Fig. 3. (a) Simulated transient magnetization, SOT voltage, and STT voltage in the P to AP switching. (i)~(v) represent the five phases of magnetization dynamics in Fig. 2(a)~(e), accordingly. The t_{SW} is defined as the time that magnetization completes 90% switching. (b) Domain images of FL during the switching.

III. Result and Discussion

The critical voltage of SOT channel ($V_{C,\,SOT}$) and $J_{C,\,SOT}$ can be extracted **(Fig. 4)**. The $J_{C,\,SOT}$ dramatically increases when the t_{SOT} is shorter than 1 ns **(Fig. 5)**. For t_{SOT} of 0.2 ns, $J_{C,\,SOT}$ is

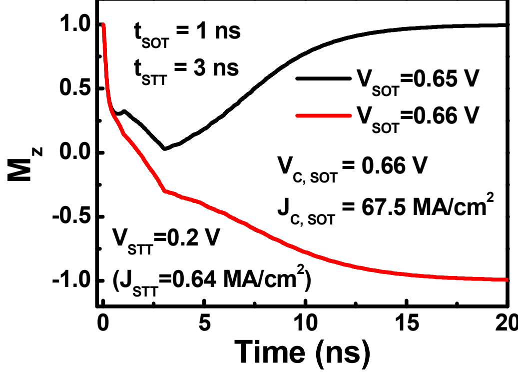

Fig. 4. Transient M_z to extract $V_{C, SOT}$ and $J_{C, SOT}$. The $V_{C, SOT}$ is defined as the minimum voltage across the SOT channel that is needed to switch the FL. The $J_{C, SOT}$ is equal to $V_{SOT}/(R_{SOT}W_{SOT}t_{SOT})$, where R_{SOT} is the resistance of the SOT channel.

reduced by 36% as the J_{STT} increases from 0.64 MA/cm^2 to 0.97 MA/cm^2. The $J_{C, SOT}$ reduction by the increasing J_{STT} (V_{STT}) is prominent at short t_{SOT}. For a short t_{SOT} (< 1 ns), the magnetization of FL cannot move close to +y axis when V_{SOT} is off due to time limitation **(Fig. 6(a))**. Since the damping torque (τ_D) is proportional to $\vec{H}_{effz}$, the spin transfer torque (τ_{STT}) proportional to J_{STT} needs to be large enough to exceed

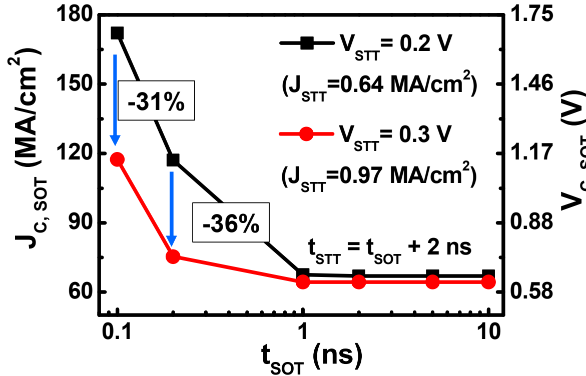

Fig. 5. $J_{C, SOT}$ vs t_{SOT} with different V_{STT}. The t_{STT} is fixed to be 2 ns longer than t_{SOT} to ensure deterministic switching.

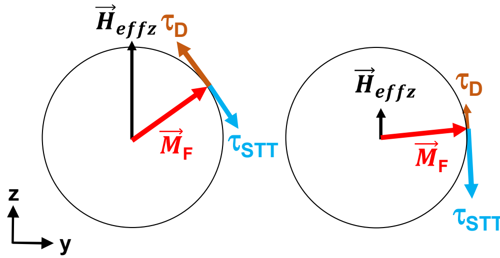

Fig. 6. Analysis of $\vec{M}_F$, $\vec{H}_{eff}$, and torque at t = t_{SOT} for (a) short t_{SOT} (< 1 ns) and (b) long t_{SOT} (≥ 1 ns).

the large τ_D. As a result, the J_{STT} dependence on $J_{C, SOT}$ is significant at short t_{SOT} **(Fig. 5)**. For a long t_{SOT} (≥ 1 ns), the magnetization has sufficient time to align close to +y axis **(Fig. 6(b))**. The small $\vec{H}_{effz}$ results in small τ_D. Therefore, the required J_{STT} (V_{STT}) to switch is small, and the J_{STT} dependence is insignificant **(Fig. 5)**.

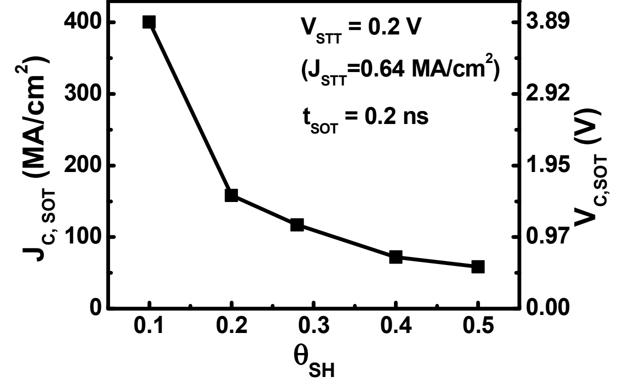

Fig. 7. $J_{C, SOT}$ with various θ_{SH} of SOT channels.

The increasing θ_{SH} decreases the $J_{C, SOT}$ due to the improved charge-to-spin conversion efficiency **(Fig. 7)**. The $J_{C, SOT}$ reduction is observed from t_{SOT} of 0.1 ns to 10 ns **(Fig. 8)**. For the t_{SOT} of 0.2 ns, the $J_{C\ SOT}$ can further be reduced by 46% as the θ_{SH} increases from 0.28 to 0.5 **(Fig. 8)**. The decreasing SOT channel current density (J_{SOT}) to write p-SOT-MTJ causes the

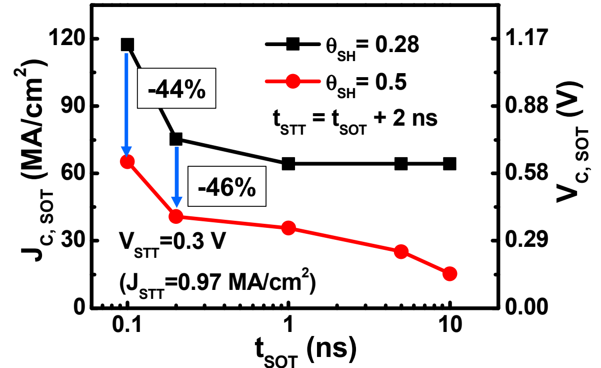

Fig. 8. $J_{C, SOT}$ vs t_{SOT} with different θ_{SH}.

t_{SW} increase **(Fig. 9)**. The large write current density is required for fast switching. However, the large write current density results in the large footprint of the access transistor, which degrades the memory density due to the large cell size. The increasing θ_{SH} and J_{STT} can lower the t_{SW} at the same J_{SOT}. With the large θ_{SH} (0.5) and J_{STT} (0.97 MA/cm^2), the t_{SW} can be reduced 60% at J_{SOT} of 120 MA/cm^2. The low $J_{C, SOT}$ (80 MA/cm^2) is obtained at t_{SW} of 5 ns **(Fig. 9)**.

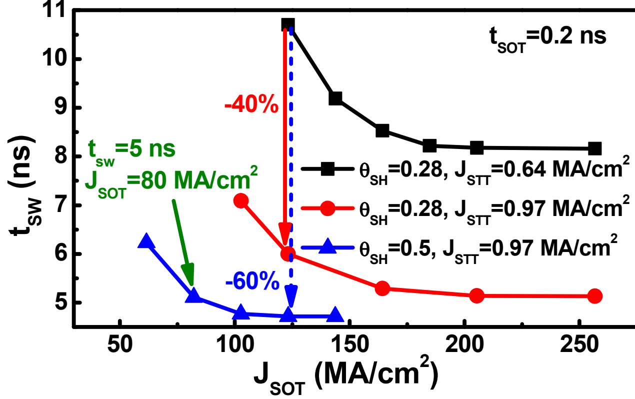

Fig. 9. t_{SW} vs J_{SOT} with different θ_{SH} and J_{STT}. The t_{SW} is defined

IV. Conclusion

The field-free switching of p-SOT-MTJ can be achieved by adding STT pulse to break the symmetry. The $J_{C, SOT}$ of p-SOT-MTJ increases with the deceasing t_{SOT}. The $J_{C, SOT}$ can be reduced by the increasing J_{STT} and θ_{SH}. The effect of J_{STT} is prominent at short t_{SOT} region. The low $J_{C, SOT}$ results in the small footprint of access transistors for the high density of SOT-MRAM.

Acknowledgment

This work is supported in part by MOST, Taiwan (109-2622-8-002-003-, 110-2218-E-002-030-, and 110-2218-E-002-034-MBK), and by MOE, Taiwan (NTU-CC-110L892601). The support of Taiwan Semiconductor Research Institute, Dr. Denny D. Tang, Prof. Jack Yuan-Chen Sun, and Fujitsu Ltd. are also appreciated.

References

[1] K. Garello, F. Yasin, H. Hody, S. Couet, L. Souriau, S. H. Sharifi, J. Swerts, R. Carpenter, S. Rao, W. Kim, J. Wu, K. K. V. Sethu, M. Pak, N. Jossart, D. Crotti, A. Furnémont, and G. S. Kar, "Manufacturable 300mm platform solution for field-free switching SOT-MRAM," *Proc. Symp. VLSI Technol.*, pp. T194-T195, 2019.

[2] S. Fukami, T. Anekawa, A. Ohkawara, C. Zhang, and H. Ohno, "A sub-ns three-terminal spin-orbit torque induced switching device," *Proc. Symp. VLSI Technol.*, pp. 1-2, 2016.

[3] N. Sato, G. A. Allen, W. P. Benson, B. Buford, A. Chakraborty, M. Christenson1, T. A. Gosavi, P. E. Heil, N. A. Kabir, B. J. Krist, K. P. O'Brien, K. Oguz, R. R. Patil, J. Pellegren, A. K. Smith, E. S. Walker, P. J. Hentges, M. V. Metz, M. Seth, B. Turkot, C.J. Wiegand, H.-J. Yoo, and I. A. Young, "CMOS Compatible Process Integration of SOT-MRAM with Heavy-Metal Bi-Layer Bottom Electrode and 10ns Field-Free SOT Switching with STT Assist," *Proc. Symp. VLSI Technol.*, pp. 1-2, 2020.

[4] B. Zeinali, J. K. Madsen, P. Raghavan and F. Moradi, "Ultra-Fast SOT-MRAM Cell with STT Current for Deterministic Switching," *IEEE International Conference on Computer Design (ICCD)*, pp. 463-468, 2017.

[5] M. Wang, W. Cai, D. Zhu, Z. Wang, J. Kan, Z. Zhao, K. Cao, Z. Wang, Y. Zhang, T. Zhang, C. Park, J.-P. Wang, A. Fert, and W. Zhao, "Field-free switching of a perpendicular magnetic tunnel junction through the interplay of spin-orbit and spin-transfer torques," *Nature Electronics*, vol. 1, pp. 582-588, 2018.

[6] H. Sato, M. Yamanouchi, K. Miura, S. Ikeda, R. Koizumi, F. Matsukura, and H. Ohno, "CoFeB Thickness Dependence of Thermal Stability Factor in CoFeB/MgO Perpendicular Magnetic Tunnel Junctions," in *IEEE Magnetics Letters*, vol. 3, pp. 3000204-3000204, 2012.

[7] H. Sato, M. Yamanouchi, K. Miura, S. Ikeda, H. D. Gan, K. Mizunuma, R. Koizumi, F. Matsukura, and H. Ohno, "Junction size effect on switching current and thermal stability in CoFeB/MgO perpendicular magnetic tunnel junctions," *Appl. Phy. Lett.*, vol. 99, no. 4, pp. 042501, 2011.

[8] Y.-J. Tsou, K.-S. Li, J.-M. Shieh, W.-J. Chen, H.-C. Chen, Y.-J. Chen, C.-L. Hsu, Y.-M. Huang, F.-K. Hsueh, W.-H. Huang, W.-K. Yeh, H.-C. Shih, P.-C. Liu, C. W. Liu, Y.-S. Yen, C.-H. Lai, J.-H. Wei, D. D. Tang, and J. Y.-C. Sun, "First Demonstration of Interface-Enhanced SAF Enabling 400ºC-Robust 42 nm p-SOT-MTJ Cells with STT-Assisted Field-Free Switching and Composite Channels," *Proc. Symp. VLSI Technol.*, 2021.

[9] S. Ikeda, K. Miura, H. Yamamoto, K. Mizunuma, H. D. Gan, M. Endo, S. Kanai, J. Hayakawa, F. Matsukura, and H. Ohno, "A perpendicular-anisotropy CoFeB–MgO magnetic tunnel junction," *Nature Mater.*, vol. 9, pp. 721-724, 2010.

[10] K. Watanabe, S. Fukami, H. Sato, F. Matsukura, and H. Ohno, "Magnetic Properties of CoFeB–MgO Stacks With Different Buffer-Layer Materials (Ta or Mo)," in *IEEE Transactions on Magnetics*, vol. 52, no. 7, pp. 1-4, 2016.

[11] R. C. O'Handley, *Modern Magnetic Materials Principles and Applications*, Wiley-Interscience, 1999.

[12] M. Voto, L. Lopez-Diaz and L. Torres, "Effects of grain size and disorder on domain wall propagation in CoFeB thin films," J. Phys. D: Appl. Phys., vol. 49, no. 18, pp. 185001, 2016.